
Scalable Multi-Task Gaussian Process Tensor Regression for Normative Modeling of Structured Variation in Neuroimaging Data

Seyed Mostafa Kia
RadboudUMC,
Donders Institute,
Nijmegen, 6525 EN
s.kia@donders.ru.nl

Christian F. Beckmann
RadboudUMC,
Donders Institute,
University of Oxford
c.beckmann@donders.ru.nl

Andre F. Marquand
RadboudUMC,
Donders Institute,
King's College London
a.marquand@donders.ru.nl

Abstract

Most brain disorders are very heterogeneous in terms of their underlying biology and developing analysis methods to model such heterogeneity is a major challenge. A promising approach is to use probabilistic regression methods to estimate normative models of brain function using (f)MRI data then use these to map variation across individuals in clinical populations (*e.g.*, via anomaly detection). To fully capture individual differences, it is crucial to statistically model the patterns of correlation across different brain regions and individuals. However, this is very challenging for neuroimaging data because of high-dimensionality and highly structured patterns of correlation across multiple axes. Here, we propose a general and flexible multi-task learning framework to address this problem. Our model uses a tensor-variate Gaussian process in a Bayesian mixed-effects model and makes use of Kronecker algebra and a low-rank approximation to scale efficiently to multi-way neuroimaging data at the whole brain level. On a publicly available clinical fMRI dataset, we show that our computationally affordable approach substantially improves detection sensitivity over both a mass-univariate normative model and a classifier that –unlike our approach– has full access to the clinical labels.

1 Introduction

Recently, there has been great interest in applying machine learning methods to quantitative biological measures (biomarkers) to assist medical decision making; for example assisting diagnosis or predicting treatment outcome in the spirit of *precision medicine* [22]. In psychiatry, this is very challenging because diagnosis is typically based on clinical symptoms and the underlying biology is highly heterogeneous [23, 16]. For example, subjects with the same diagnosis may have different underlying biological defects. Most research ignores such heterogeneity and instead treats groups as distinct entities (*e.g.*, a case-control approach where subjects are either "patients" or "controls") [8]. Supervised machine learning methods applied to neuroimaging data have been widely used for this but their accuracy is fundamentally limited by the heterogeneity within each disorder [34], therefore, there is an urgent need to go beyond case-control settings. Normative modeling [21] is one promising approach for this that aims to characterize variation across a healthy cohort before making predictions so that subjects that deviate from the resulting *normative* model can be detected as outliers in an anomaly detection setting and the pattern underlying the deviation can be further analyzed to understand the biological underpinnings.

Neuroimaging techniques provide detailed measures of the brain structure and function and excellent candidate biomarkers for brain disorders. However, these data present substantial challenges including: i) variability along multiple axes including across different individuals, brain locations, and cognitive

systems [13]; ii) high dimensionality, where a large number of measurements (order of 10^{5-6}) are acquired from multiple subjects (usually order of 10^{2-3}); iii) strong correlations within and across data axes (*e.g.*, brain locations). There is a pressing need to develop methods that can model such complex covariance structures and that scale reasonably with increasing computational demands.

Gaussian process regression [31] (GPR) is an established method for modeling such correlations. For example, the GPR was used to model variation across subjects, where estimates of predictive confidence quantify centiles of variation in the population [21]. However, this was done in a mass-univariate fashion, ignoring correlations between sampled brain locations (voxels or vertices). Since abnormalities may be encoded via correlations between variables, this approach is suboptimal. GPR is also widely used in spatial statistics, but is limited to small datasets because of the need to invert the spatial covariance matrix. Indeed, in neuroimaging, spatial models are very computationally demanding because of the need to invert large covariance matrices across space, subjects or both [6]. Whilst the classic GPR approach aims to model only a single output variable, it can be extended to multi-task GPR [5] (MT-GPR) to jointly predict multiple outputs. Here, we adopt a multi-task learning framework to enable the model to capitalize on the structure in the output space. This provides a natural approach to model correlations across samples and output variables (*e.g.*, voxels). However, MT-GPR comes with extra computational overheads in time and memory requirements. Although various approaches have been proposed to improve computational efficiency based on approximations [2, 4, 3] or utilizing properties of Kronecker product [29, 26], MT-GPR remains computationally intractable in processing neuroimaging data at the whole-brain level.

In this paper, we make three contributions: i) we propose a general and versatile method called *scalable multi-task Gaussian process tensor regression* (sMT-GPTR) to extend GPR to predict hundreds of thousands of tasks simultaneously. This is based on a tensor-variate normal distribution [10] and generalizes previous approaches that use a Kronecker product covariance structure (*e.g.*, the "GP-Kronsum" [26] approach); ii) we propose a fast inference algorithm where we employ tensor factorization techniques [24] to provide a low-rank approximation of the high-dimensional task covariance matrix and further exploit algebraic properties of the Kronecker product [20]; iii) we apply this to multi-way neuroimaging data to jointly accommodate multiple axes of variation (*e.g.*, spatial variation, and variation across subjects and covariates). For this, we predict task-related functional MRI brain activity from a set of clinical covariates (*e.g.*, symptom scores) in a mixed-effects model [9]. This can be seen as a generalization of previous approaches such as the spatial Gaussian predictive process (SGPP) framework [14, 15]. We refer to this generalization as a *tensor Gaussian predictive process* (TGPP). This framework provides multiple advantages: it allows us to jointly predict multiple output dimensions, accounting for correlations within and across dimensions and potentially heteroscedastic noise structures. Our approach also has reasonable time and storage complexities and scales to high-dimensional (*i.e.*, whole brain) neuroimaging data. It can also easily be extended to handle additional sources of variation (*e.g.*, across timepoints or data modalities). We evaluate this method on a publicly available clinical fMRI dataset [25], and show that: i) the proposed sMT-GPTR approach is effective in modeling variation across both space and subjects in a healthy human cohort using whole-brain neuroimaging data; ii) in a normative modeling context [21] the proposed method more accurately identifies psychiatric patients from healthy individuals, whilst iii) provides focal neural signatures of the underlying abnormalities.

2 Methods

2.1 Notation

In this text, we use respectively calligraphic capital letters, \mathcal{A} , boldface capital letters, \mathbf{A} , and capital letters, A , to denote tensors, matrices, and scalar numbers. We denote the vertical vector which results from collapsing a matrix \mathbf{A} or tensor \mathcal{A} with $\text{vec}(\mathbf{A})$ or $\text{vec}(\mathcal{A})$, respectively. We denote an identity matrix by \mathbf{I} ; and the determinant, diagonal elements, and the trace of matrix \mathbf{A} with $|\mathbf{A}|$, $\text{diag}(\mathbf{A})$, and $\text{Tr}[\mathbf{A}]$, respectively. We use \otimes , \odot , and \times_n to respectively denote Kronecker, element-wise, and n -mode tensor products. The i -mode matricized version of a tensor $\mathcal{A} \in \mathbb{R}^{I_1 \times \dots \times I_D}$ is shown as $\mathbf{A}_{(i)} \in \mathbb{R}^{I_i \times I_1 \dots I_{i-1} \cdot I_{i+1} \dots I_D}$. We use concise notation $\mathbf{A}_i \mid_{i=1}^D$ and $\bigotimes_{i=1}^D \mathbf{A}_i$ for $\mathbf{A}_1, \dots, \mathbf{A}_D$ and $\mathbf{A}_1 \otimes \dots \otimes \mathbf{A}_D$, respectively. We use $\mathbf{A}[i, j]$, $\mathbf{A}[:, i]$, and $\mathbf{A}[i, :]$ to respectively refer to a certain element and a row or column vector in a matrix \mathbf{A} (similar for a tensor \mathcal{A}).

2.2 Tensor Gaussian Predictive Process for Modeling Neuroimaging Data

Consider a neuroimaging study with N subjects and let $\mathbf{X} \in \mathbb{R}^{N \times F}$ to denote the design matrix of F covariates of interest for N subjects (*e.g.*, demographic, cognitive, or neurophysiological covariates). Let $\mathcal{Y} \in \mathbb{R}^{N \times T_1 \times \dots \times T_D}$ to represent a $(D+1)$ -order tensor of multivariate neuroimaging data for corresponding N subjects. In this text, we refer to D as the number of dimensions of multi-way neuroimaging data. For example in the case of volumetric structural MRI, we have $D = 3$ where each dimension refers to x , y , and z axis, hence \mathcal{Y} is a 4-order tensor with T_1 , T_2 , and T_3 voxels in corresponding data dimensions. From the theoretical perspective, we put no restriction on the order of \mathcal{Y} and it could take any value between 2 to an arbitrary natural number. This makes the presented methodology more flexible for different neuroimaging modalities (*e.g.*, structural/functional MRI) and study designs (*e.g.*, longitudinal studies, multiple contrast data). Extending Gaussian predictive process models [14, 15] and as a generalization of the general linear model (GLM) to multi-way data structures, we define the tensor Gaussian predictive process (TGPP) as follows:

$$\mathcal{Y} = \mathbf{X} \times_1 \mathcal{A} + \mathcal{Z} + \mathcal{E}, \quad (1)$$

where $\mathcal{A} \in \mathbb{R}^{F \times T_1 \times \dots \times T_D}$ is a $(D+1)$ -order tensor that contains regression coefficients estimated by solving the following linear equations (for example using ordinary least squares regression):

$$\hat{\mathcal{Y}}[:, i, \dots, j] = \mathbf{X} \mathcal{A}[:, i, \dots, j], \quad \text{for } i = 1, \dots, T_1; \dots; \text{for } j = 1, \dots, T_D. \quad (2)$$

Here, \mathcal{A} represents the *fixed-effect* across subjects. On the other hand, $\mathcal{Z} \in \mathbb{R}^{N \times T_1 \times \dots \times T_D}$ represents the *random-effect* that characterizes the joint variations from the fixed-effect across different dimensions of neuroimaging data in \mathcal{Y} (*e.g.*, across different individuals, spatio-temporal measures, or modalities). Finally, $\mathcal{E} \in \mathbb{R}^{N \times T_1 \times \dots \times T_D}$ is multivariate noise. We assume a zero-mean tensor-variate normal distribution, as a generalization of the matrix normal distribution, for \mathcal{Z} and \mathcal{E} :

$$p(\mathcal{Z} \mid \mathbf{D}_i \mid_{i=1}^D, \mathbf{R}) = \mathcal{TN}(\mathbf{0}, \bigotimes_{i=1}^D \mathbf{D}_i \otimes \mathbf{R}) = \frac{\exp(-\frac{1}{2} \text{vec}(\mathcal{Z})^\top [\bigotimes_{i=1}^D \mathbf{D}_i \otimes \mathbf{R}]^{-1} \text{vec}(\mathcal{Z}))}{\sqrt{(2\pi)^{NT} \left| \bigotimes_{i=1}^D \mathbf{D}_i \right|^T |\mathbf{R}|^N}}, \quad (3a)$$

$$p(\mathcal{E} \mid \mathbf{\Xi}_i \mid_{i=1}^D, \mathbf{\Omega}) = \mathcal{TN}(\mathbf{0}, \bigotimes_{i=1}^D \mathbf{\Xi}_i \otimes \mathbf{\Omega}) = \frac{\exp(-\frac{1}{2} \text{vec}(\mathcal{E})^\top [\bigotimes_{i=1}^D \mathbf{\Xi}_i \otimes \mathbf{\Omega}]^{-1} \text{vec}(\mathcal{E}))}{\sqrt{(2\pi)^{NT} \left| \bigotimes_{i=1}^D \mathbf{\Xi}_i \right|^T |\mathbf{\Omega}|^N}}, \quad (3b)$$

where $T = \prod_{i=1}^D T_i$, and $\mathbf{R}, \mathbf{\Omega} \in \mathbb{R}^{N \times N}$ are respectively covariance matrices of \mathcal{Z} and \mathcal{E} across subjects; $\mathbf{D}_i, \mathbf{\Xi}_i \in \mathbb{R}^{T_i \times T_i}$ represent the covariance matrices of random-effect and noise terms across i th dimension of data, *i.e.*, i -mode covariance matrices of \mathcal{Z} and \mathcal{E} . Based on this assumption on the distribution of \mathcal{Z} and \mathcal{E} , we generalize sum of Kronecker products covariance structure (GP-Kronsum) approach [26] to the multi-task Gaussian process tensor regression (MT-GPTR) to jointly estimate parameters of $\mathbf{R}, \mathbf{\Omega}, \mathbf{D}_i$, and $\mathbf{\Xi}_i$ in a multi-way representation of neuroimaging data:

$$p(\text{vec}(\mathcal{Z} + \mathcal{E}) \mid \mathbf{X}, \mathbf{D}_i \mid_{i=1}^D, \mathbf{R}, \mathbf{\Xi}_i \mid_{i=1}^D, \mathbf{\Omega}) = \mathcal{GP}(\text{vec}(\mathcal{Y} - \hat{\mathcal{Y}}) \mid \mathbf{0}, \bigotimes_{i=1}^D \mathbf{D}_i \otimes \mathbf{R} + \bigotimes_{i=1}^D \mathbf{\Xi}_i \otimes \mathbf{\Omega}). \quad (4)$$

Here \mathbf{R} and $\mathbf{\Omega}$ are defined in the input space \mathbf{X} in a multi-task setting [5]. Considering the inherent high dimensionality of neuroimaging data, computing the inverse covariance matrix in Eq. 4 is computationally expensive, thus there is a pressing need to reduce the time and space complexities of MT-GPTR. In the following, we combine the tensor factorization technique with elegant properties of Kronecker product [20] in order to extend the application of MT-GPTR to large output spaces.

2.3 Scalable Multi-Task Gaussian Process Tensor Regression (sMT-GPTR)

Let $\Phi: \mathcal{Y} - \hat{\mathcal{Y}} \rightarrow \mathcal{Z}'$ be an orthogonal linear transformation that transforms $\mathcal{Z} + \mathcal{E}$ to a reduced latent space $\mathcal{Z}' \in \mathbb{R}^{N \times P_1 \times \dots \times P_D}$, where $P_i < T_i$. A tensor factorization technique [18] can be used for this transformation wherein $\mathcal{Z} + \mathcal{E} \approx \hat{\mathcal{Z}} = \mathcal{Z}' \times_2 \mathbf{B}_1 \times_3 \dots \times_{D+1} \mathbf{B}_D$. Here, columns of $\mathbf{B}_i \in \mathbb{R}^{T_i \times P_i}$ represent a set of P_i orthogonal basis functions across the i th dimension of data. Assuming a zero-mean tensor normal distribution for \mathcal{Z}' , we have (see supplement for the derivation):

$$p(\mathcal{Z}' \mid \mathbf{C}_i \mid_{i=1}^D, \mathbf{R}) = \mathcal{TN}(\mathbf{0}, \bigotimes_{i=1}^D \mathbf{C}_i \otimes \mathbf{R}) = \frac{\exp(-\frac{1}{2} \text{Tr}[\bigotimes_{i=1}^D \mathbf{B}_i \mathbf{C}_i^{-1} \mathbf{B}_i^\top \hat{\mathbf{Z}}_{(1)}^\top \mathbf{R}^{-1} \hat{\mathbf{Z}}_{(1)}])}{\sqrt{(2\pi)^N \prod_{i=1}^D P_i \left| \bigotimes_{i=1}^D \mathbf{C}_i \right|^{\prod_{i=1}^D P_i} |\mathbf{R}|^N}}, \quad (5)$$

where $\mathbf{C}_i \in \mathbb{R}^{P_i \times P_i}$ is the i -mode covariance matrix in the reduced latent space. Interestingly, we have $p(\mathcal{Z}' \mid \mathbf{C}_i \mid_{i=1}^D, \mathbf{R}) = p(\hat{\mathcal{Z}} \mid \mathbf{B}_i \mathbf{C}_i \mathbf{B}_i^\top \mid_{i=1}^D, \mathbf{R})$. Assuming $\hat{\mathcal{Z}}$ to explain the majority of the variance in the random-effect, we use the numerator in Eq. 5 as an approximation for the numerator in Eq. 3a, thus:

$$p(\mathcal{Z} \mid \mathbf{D}_i \mid_{i=1}^D, \mathbf{R}) \approx p(\hat{\mathcal{Z}} \mid \mathbf{B}_i \mathbf{C}_i \mathbf{B}_i^\top \mid_{i=1}^D, \mathbf{R}) \quad , \quad (6)$$

where \mathbf{D}_i is approximated by $\mathbf{B}_i \mathbf{C}_i \mathbf{B}_i^\top$. Analogously, using $\mathcal{Y} - \hat{\mathcal{Y}} - \hat{\mathcal{Z}}$ as a proxy for \mathcal{E} and setting $\mathcal{Y} - \hat{\mathcal{Y}} - \hat{\mathcal{Z}} \approx \hat{\mathcal{E}} = \mathcal{E}' \times_2 \mathbf{\Lambda}_1 \times_3 \cdots \times_{D+1} \mathbf{\Lambda}_D$, for $\mathbf{\Lambda}_i \in \mathbb{R}^{T_i \times Q_i}$, and assuming a zero-mean tensor normal distribution on \mathcal{E}' we have:

$$p(\mathcal{E} \mid \mathbf{\Xi}_i \mid_{i=1}^D, \mathbf{\Omega}) \approx p(\hat{\mathcal{E}} \mid \mathbf{\Lambda}_i \mathbf{\Sigma}_i \mathbf{\Lambda}_i^\top \mid_{i=1}^D, \mathbf{\Omega}) \quad . \quad (7)$$

Based on Eq. 6 and Eq. 7, our scalable multi-task Gaussian process tensor regression (sMT-GPTR) model can be derived in the latent space by rewriting Eq. 4 using approximated covariance matrices:

$$\begin{aligned} & p(\text{vec}(\mathcal{Z} + \mathcal{E}) \mid \mathbf{X}, \mathbf{D}_i \mid_{i=1}^D, \mathbf{R}, \mathbf{\Xi}_i \mid_{i=1}^D, \mathbf{\Omega}) \approx \\ & p(\text{vec}(\hat{\mathcal{Z}} + \hat{\mathcal{E}}) \mid \mathbf{X}, \mathbf{C}_i \mid_{i=1}^D, \mathbf{B}_i \mid_{i=1}^D, \mathbf{R}, \mathbf{\Sigma}_i \mid_{i=1}^D, \mathbf{\Lambda}_i \mid_{i=1}^D, \mathbf{\Omega}) = \\ & \mathcal{GP}(\text{vec}(\mathcal{Y} - \hat{\mathcal{Y}}) \mid \mathbf{0}, \bigotimes_{i=1}^D \mathbf{B}_i \mathbf{C}_i \mathbf{B}_i^\top \otimes \mathbf{R} + \bigotimes_{i=1}^D \mathbf{\Lambda}_i \mathbf{\Sigma}_i \mathbf{\Lambda}_i^\top \otimes \mathbf{\Omega}). \end{aligned} \quad (8)$$

2.3.1 Predictive Distribution

Following the standard GPR framework [31], the mean and variance of the predictive distribution of sMT-GPTR in Eq. 8 on N^* test samples, *i.e.*, $p(\text{vec}(\mathcal{Y}^*) - \text{vec}(\hat{\mathcal{Y}}^*) \mid \text{vec}(\mathcal{M}^*), \mathbf{V}^*)$, in which $\mathbf{V}^* \in \mathbb{R}^{N^* T \times N^* T}$, can be computed as follows:

$$\text{vec}(\mathcal{M}^*) = (\bigotimes_{i=1}^D \mathbf{B}_i \mathbf{C}_i \mathbf{B}_i^\top \otimes \mathbf{R}^*) (\bigotimes_{i=1}^D \mathbf{B}_i \mathbf{C}_i \mathbf{B}_i^\top \otimes \mathbf{R} + \bigotimes_{i=1}^D \mathbf{\Lambda}_i \mathbf{\Sigma}_i \mathbf{\Lambda}_i^\top \otimes \mathbf{\Omega})^{-1} \text{vec}(\mathcal{Y}), \quad (9a)$$

$$\begin{aligned} \mathbf{V}^* &= (\bigotimes_{i=1}^D \mathbf{B}_i \mathbf{C}_i \mathbf{B}_i^\top \otimes \mathbf{R}^{**}) - (\bigotimes_{i=1}^D \mathbf{B}_i \mathbf{C}_i \mathbf{B}_i^\top \otimes \mathbf{R}^*) \\ & \quad (\bigotimes_{i=1}^D \mathbf{B}_i \mathbf{C}_i \mathbf{B}_i^\top \otimes \mathbf{R} + \bigotimes_{i=1}^D \mathbf{\Lambda}_i \mathbf{\Sigma}_i \mathbf{\Lambda}_i^\top \otimes \mathbf{\Omega})^{-1} (\bigotimes_{i=1}^D \mathbf{B}_i \mathbf{C}_i \mathbf{B}_i^\top \otimes \mathbf{R}^{*\top}), \end{aligned} \quad (9b)$$

where $\mathbf{R}^{**} \in \mathbb{R}^{N^* \times N^*}$ is the covariance matrix of test samples, and $\mathbf{R}^* \in \mathbb{R}^{N^* \times N}$ is the cross-covariance matrix between the test and training samples. Employing sMT-GPTR enables us to estimate structured epistemic and aleatoric uncertainties in the output space [17]. Specifically, elements in $\text{diag}(\mathbf{V}^*)$ can be rearranged into the predictive variance tensor $\mathcal{V}^* \in \mathbb{R}^{N \times T_1 \times \cdots \times T_D}$ reflecting the epistemic uncertainty in predictions (*i.e.*, parameter uncertainty that can be reduced given more data). On the other hand, elements in $\text{diag}(\mathbf{\Lambda}_i \mathbf{\Sigma}_i \mathbf{\Lambda}_i^\top)$ can be rearranged into a tensor $\mathcal{U} \in \mathbb{R}^{T_1 \times \cdots \times T_D}$ reflecting aleatoric uncertainty (*i.e.*, noise in the data).

2.3.2 Efficient Prediction and Optimization

For efficient prediction and fast optimization of the log-likelihood, we extend the efficient optimization and prediction procedures proposed in [26] to cope with our reduced latent space formulations. To this end, we exploit properties of Kronecker product and the eigenvalue decomposition for diagonalizing the covariance matrices in the reduced latent space. Based on our assumption on the orthogonality of components in \mathbf{B}_i , we set $\mathbf{B}_i^{-1} = \mathbf{B}_i^\top$ and $\mathbf{B}_i^\top \mathbf{B}_i = \mathbf{I}$ (and equivalently for $\mathbf{\Lambda}_i$), in sequel, the predictive mean and variance can be efficiently computed by (see supplementary for details):

$$\mathbf{M}_{(1)}^* = \mathbf{R}^* \mathbf{U}_\Omega \mathbf{S}_\Omega^{-0.5} \mathbf{U}_{\tilde{\mathbf{R}}}^\top \tilde{\mathbf{Y}} \bigotimes_{i=1}^D \mathbf{U}_{\tilde{\mathbf{C}}_i}^\top \mathbf{S}_{\tilde{\mathbf{\Sigma}}_i}^{-0.5} \mathbf{U}_{\tilde{\mathbf{\Sigma}}_i}^\top \mathbf{\Lambda}_i^\top \mathbf{B}_i \mathbf{C}_i \mathbf{B}_i^\top, \quad (10a)$$

$$\begin{aligned} \mathbf{V}^* &= (\bigotimes_{i=1}^D \mathbf{B}_i \mathbf{C}_i \mathbf{B}_i^\top \otimes \mathbf{R}^{**}) - (\bigotimes_{i=1}^D \mathbf{B}_i \mathbf{C}_i \mathbf{B}_i^\top \mathbf{\Lambda}_i \mathbf{U}_{\tilde{\mathbf{\Sigma}}_i} \mathbf{S}_{\tilde{\mathbf{\Sigma}}_i}^{-0.5} \mathbf{U}_{\tilde{\mathbf{C}}_i}^\top \otimes \mathbf{R}^* \mathbf{U}_\Omega \mathbf{S}_\Omega^{-0.5} \mathbf{U}_{\tilde{\mathbf{R}}}^\top) \\ & \quad (\bigotimes_{i=1}^D \mathbf{S}_{\tilde{\mathbf{C}}_i} \otimes \mathbf{S}_{\tilde{\mathbf{R}}} + \mathbf{I})^{-1} (\bigotimes_{i=1}^D \mathbf{U}_{\tilde{\mathbf{C}}_i}^\top \mathbf{S}_{\tilde{\mathbf{\Sigma}}_i}^{-0.5} \mathbf{U}_{\tilde{\mathbf{\Sigma}}_i}^\top \mathbf{\Lambda}_i^\top \mathbf{B}_i \mathbf{C}_i \mathbf{B}_i^\top \otimes \mathbf{U}_{\tilde{\mathbf{R}}}^\top \mathbf{S}_\Omega^{-0.5} \mathbf{U}_\Omega \mathbf{R}^{*\top}), \end{aligned} \quad (10b)$$

where in these efficient formulations we have $vec(\tilde{\mathbf{Y}}) = diag[(\bigotimes_{i=1}^D \mathbf{S}_{\tilde{\mathbf{C}}_i} \otimes \mathbf{S}_{\tilde{\mathbf{R}}} + \mathbf{I})^{-1}] \odot vec(\mathbf{Y}')$, $\mathbf{Y}' = \mathbf{U}_{\tilde{\mathbf{R}}}^\top \mathbf{S}_{\Omega}^{-0.5} \mathbf{U}_{\Omega}^\top \mathbf{Y}_{(1)} \bigotimes_{i=1}^D \mathbf{\Lambda}_i \mathbf{U}_{\Sigma_i} \mathbf{S}_{\Sigma_i}^{-0.5} \mathbf{U}_{\tilde{\mathbf{C}}_i}^\top$, $\tilde{\mathbf{C}}_i = \mathbf{S}_{\Sigma_i}^{-0.5} \mathbf{U}_{\Sigma_i}^\top \mathbf{\Lambda}_i^\top \mathbf{B}_i \mathbf{C}_i \mathbf{B}_i^\top \mathbf{\Lambda}_i \mathbf{U}_{\Sigma_i} \mathbf{S}_{\Sigma_i}^{-0.5}$, and $\tilde{\mathbf{R}} = \mathbf{S}_{\Omega}^{-0.5} \mathbf{U}_{\Omega}^\top \mathbf{R} \mathbf{U}_{\Omega} \mathbf{S}_{\Omega}^{-0.5}$. Here $\Sigma_i = \mathbf{U}_{\Sigma_i} \mathbf{S}_{\Sigma_i} \mathbf{U}_{\Sigma_i}^\top$ and $\Omega = \mathbf{U}_{\Omega} \mathbf{S}_{\Omega} \mathbf{U}_{\Omega}^\top$ are eigenvalue decomposition of covariance matrices (similar for $\tilde{\mathbf{C}}_i$ and $\tilde{\mathbf{R}}$). Note that in the new parsimonious formulation for the prediction mean, heavy time and space complexities of computing the inverse kernel matrix is reduced to computing the inverse of a diagonal matrix, *i.e.*, reciprocals of diagonal elements of $\bigotimes_{i=1}^D \mathbf{S}_{\tilde{\mathbf{C}}_i} \otimes \mathbf{S}_{\tilde{\mathbf{R}}} + \mathbf{I}$. For the predictive variance, explicit computation of the Kronecker product is still necessary but the required time and storage can be significantly reduced by computing only diagonal members of \mathbf{V}^* in mini-batches. To efficiently evaluate the negative log-marginal likelihood of Eq. 8, we have (see supplement for derivation):

$$L = -\frac{NT}{2} \ln(2\pi) - \frac{N}{2} \sum_{j=1}^T (\ln \bigotimes_{i=1}^D \mathbf{S}_{\Sigma_i}[j, j]) - \frac{T}{2} \sum_{j=1}^N (\ln \mathbf{S}_{\Omega}[j, j]) - \frac{1}{2} \sum_{k=1}^T \sum_{j=1}^N \ln \left(\bigotimes_{i=1}^D \mathbf{S}_{\tilde{\mathbf{C}}_i}[k, k] \mathbf{S}_{\tilde{\mathbf{R}}}[j, j] + 1 \right) - \frac{1}{2} vec(\mathbf{Y}')^\top \left(\bigotimes_{i=1}^D \mathbf{S}_{\tilde{\mathbf{C}}_i} \otimes \mathbf{S}_{\tilde{\mathbf{R}}} + \mathbf{I} \right)^{-1} vec(\mathbf{Y}') \quad (11)$$

The proposed sMT-GPTR model has four sets of parameters: 1) $\Theta_{\mathbf{C}_i} \mid_{i=1}^D$, 2) $\Theta_{\Sigma_i} \mid_{i=1}^D$, 3) $\Theta_{\mathbf{R}}$, and 4) Θ_{Ω} ; which are optimized by maximizing Eq.11 (see supplementary for expressions of relevant gradients). In addition, the proposed model has two sets of hyperparameters: 1) $P_i \mid_{i=1}^D$, and 2) $Q_i \mid_{i=1}^D$; that respectively decide the number of components in $\mathbf{B}_i \mid_{i=1}^D$ and $\mathbf{\Lambda}_i \mid_{i=1}^D$. These hyperparameters should be set by means of model selection.

2.3.3 Computational Complexities

The time and space complexities of the proposed method in the optimization phase are $\mathcal{O}(N^3 + \sum_{i=1}^D P_i^3 + \sum_{i=1}^D Q_i^3 + NT^2 + N^2T)$ and $\mathcal{O}(N^2 + \sum_{i=1}^D P_i^2 + \sum_{i=1}^D Q_i^2 + NT)$, respectively. The first three terms belong to the eigenvalue decomposition of \mathbf{R} , Ω , Σ_i , and \mathbf{C}_i . The last two terms are related to the transformation of $\mathbf{Y}_{(1)}$ to \mathbf{Y}' in Eq. 11. For reasonably small P_i and Q_i ; and for a very large output space where $T \gg N$, the time and space complexities reduce to $\sim \mathcal{O}(T^2)$ and $\sim \mathcal{O}(T)$ which is one order of magnitude less than the original GP-Kronsum algorithm [26] ($\mathcal{O}(T^3)$ and $\mathcal{O}(T^2)$). Such an improvement yields substantial speed up in the case of neuroimaging data where T is generally in order of 10^5 or larger. Furthermore, due to the reasonable memory requirement, it makes the impossible mission of multi-task GPR on the whole-brain data possible.

3 Experiments and Results

3.1 Experimental Materials and Setup

As a proof of concept, we apply the proposed framework on a clinical neuroimaging dataset from the UCLA Consortium for Neuropsychiatric Phenomics [25]. The preprocessed data [12] from 119 healthy subjects and 49 individuals with schizophrenia were used in our experiments.¹ We used all covariates (\mathbf{X} with $F = 30$) from a screening instrument for psychiatric disorders (the "General Health Questionnaire"²) to predict a main task effect contrast from the "task switching" task that is known to be impaired in many clinical conditions [25] (\mathcal{Y}). This can be seen as a normative model encoding a general screening tool for psychiatric problems. We used 3D-contrast volumes ($D = 3$) derived from the standard fMRI pipeline in [12], and masked it with the group mask from the original study. Then, we cropped the volumes to the minimal bounding-box of $49 \times 61 \times 40$ voxels ($T_1 = 49, T_2 = 61, T_3 = 40, T = 119560$).

We compare sMT-GPTR with single-task GPR (ST-GPR), *i.e.*, our multivariate TGPP framework versus the mass-univariate approach, in terms of their normative modeling accuracy and runtime. Note that the comparison with other multi-task GPR approaches is not possible due to their excessive resource requirements when applied to 119560 output variables. For example, in this case GP-Kronsum [26] needs at least 80GB memory for storing the task covariance matrix. To this end, we

¹Available through the OpenfMRI project at <https://openfmri.org/dataset/ds000030/>.

²See <https://www.statisticssolutions.com/general-health-questionnaire-ghq/>

Table 1: Description and number of parameters and hyperparameters in two benchmarked methods.

Method	No. Parameters	No. Hyperparameters	Description
ST-GPR	597800	-	Parameters: $(\Theta_R + \Theta_\sigma) \times T = (4 + 1) \times 119560$
sMT-GPTR	29	6	Parameters: $ \Theta_R + \Theta_\Omega + \sum_{i=1}^3 \Theta_{C_i} + \sum_{i=1}^3 \Theta_{\Sigma_i} = 4 + 1 + 12 + 12$ Hyperparameters: $P_1, P_2, P_3, Q_1, Q_2, Q_3$

use the proposed TGPP framework in a novelty detection setting using normative modeling [21]. In this setting, we first train a model on a subset of healthy subjects and then calculate the normative probability maps (NPMs) by computing $(\mathcal{Y}_{true} - \mathcal{Y}_{pred})/\sqrt{\mathcal{S}}$ where \mathcal{Y}_{true} and \mathcal{Y}_{pred} are respectively the true and predicted outputs using Eq. 1. Here, \mathcal{S} represents the sum of epistemic and aleatoric uncertainties and we have $\mathcal{S}[i, j, k, l] = \mathcal{V}^*[i, j, k, l] + \mathcal{U}[j, k, l]$ for the i th test subject at the j, k, l th voxel in xyz MRI coordinate system. We use extreme value statistics to provide a statistical model for the deviations, as in [21]. Specifically, we use a block-maximum approach on the top 1% values in NPMs and fit these to a generalized extreme value distribution (GEVD) [7]. Then for a given test sample, we interpret the value of the cumulative distribution function of GEVD as the probability of that sample being an abnormal sample. Given these probabilities and actual labels, we evaluate the area under the ROC curve (AUC) to measure the performance of the model in distinguishing between healthy individuals from schizophrenia patients. To this end, we randomly divide the data into three subsets: 1) 39 healthy subjects to train models; 2) 39 healthy subjects to estimate the parameters of the GEVD; and 3) 41 healthy subjects and all 49 patients data in the test set. All steps (random sampling, modeling, and evaluation) are repeated 20 times in order to estimate the fluctuations of models trained on different training sets.

In all experiments, we use ordinary least squares to estimate the fixed-effect in Eq. 2. In the sMT-GPTR case, the Tucker model [30] from Tensorly package [19] is used for tensor factorization and we set correspondingly $P_1 = P_2 = P_3 = 3, 5, 10, 15$ and $Q_1 = Q_2 = Q_3 = 1, 3, 5, 10$. In all models, we use a composite covariance function of a linear, a squared exponential, and a diagonal isotropic covariance functions for \mathbf{R} , $\mathbf{C}_i \mid_{i=1}^3$, and $\Sigma_i \mid_{i=1}^3$; and a diagonal isotropic covariance function for Ω . The truncated Newton algorithm is used for optimizing the parameters. Table 1 summarizes the number of parameters and hyperparameters of two benchmarked methods. All experiments are performed using an Intel® Xeon® E5-2640 v3 @2.60GHz CPU and 16GB of RAM.³

3.2 sMT-GPTR: Faster, More Accurate, and Feasible in Whole-brain Inference

Figure 1 compares the AUC and runtime of ST-GPR with those of sMT-GPTR for different numbers of components in tensor factorization. As illustrated in Fig. 1(a), accounting for spatial structures in the signal and noise in multi-task learning provides normative models with better detection accuracy relative to single-task learning. Using sufficient components in the tensor factorization, the sMT-GPTR approach provides substantially higher accuracy in detecting abnormal samples. This gain in the novelty detection performance is even achieved by sMT-GPTR(5,3), *i.e.*, sMT-GPTR with 5 and 3 components to respectively explain the variances of the random-effect and noise, and then remains at the same level for more components. Considering the fact that ST-GPR and sMT-GPTR models showed similar regression performance (see supplement), the AUC boost in sMT-GPTR models probably reflect better estimations of epistemic and aleatoric uncertainties. The improvements can be further illustrated in a comparison with a supervised approach. Thus, we evaluated a linear support vector classifier, as is a standard practice in fMRI, in a 10-fold cross-validation setting and we achieved inferior AUC of 0.78 ± 0.04 compared to our unsupervised approach. The fact that our approach outperforms a fully supervised approach, despite never having seen a patient indicates that the target pattern is not consistent across individuals within the patient group. Instead, the normative model focuses only on estimating the healthy distribution and can detect differences from this distribution regardless of whether they are consistent with one another.

In addition to making multi-task learning possible in a very high-dimensional setting, for a reasonable number of components, sMT-GPTR is significantly faster than ST-GPR in terms of total runtime (Fig. 1(b)). For example, sMT-GPTR(10,5) is 17 times faster than ST-GPR reducing its runtime from ~ 4 hours to ~ 15 minutes. Even though the model selection process to decide the number of components is a time-consuming step in practice, due to the low running time of the proposed

³Implementations are made available online at <https://github.com/smkia/MTNorm>.

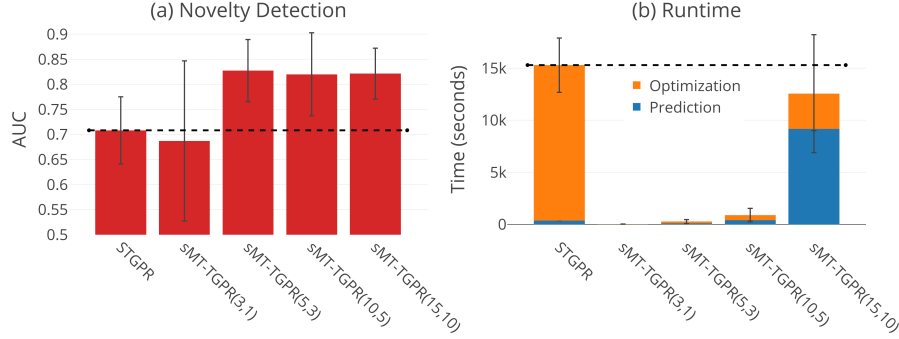


Figure 1: Comparison between ST-GPR and sMT-GPTR in terms of: a) AUC in the abnormal sample detection using normative modeling, and b) optimization and prediction runtime. The numbers in the parentheses show the number of components used in tensor factorization of $\hat{\mathcal{Z}}$ and $\hat{\mathcal{E}}$.

approach, it remains economical compared to other multi-task alternatives. In the end, it is worthwhile to emphasize that these improvements are achieved by reducing the degree-of-freedom of the normative model from 597800 for ST-GPR to 35 for sMT-GPTR (see Table 1 for the number of parameters and hyperparameters of different models).

3.3 Understanding the Underlying Neural Patterns of Abnormality

We have shown that accounting for spatial structure provides more accurate normative models than a baseline model. However, it is also important to understand the neural basis of the underlying abnormalities. To achieve this for ST-GPR and sMT-GPTR, we use a spatial mixture model [36] to translate the NPM of each subject to a probability map, where the value of each voxel represents the probability that voxel deviates from the normative model [35]. Figure 2 shows the resulting probability maps averaged across runs and the healthy/schizophrenia population in the test set.⁴ These illustrate that: i) the probability of deviating from the normative model is higher in individuals with schizophrenia than healthy subjects. This observation explains the high novelty detection rate in the case-control setting (see Figure 1(a)). Importantly, the abnormal patterns are probably not consistent across subjects in the schizophrenia group because the classifier that uses the class labels produces lower accuracy. The normative model does not require the cases to be consistent since it focuses on estimating the distribution of the controls; ii) the areas with high deviation probability are more spatially focal in sMT-GPTR models than the ST-GPR model. This suggests that the sMT-GPTR approach is better able to focus on the core abnormalities underlying the disorder and that accounting for spatial structure in both random-effect and noise provides a better estimation of epistemic and aleatoric uncertainties in sMT-GPTR models; iii) despite similar accuracy, sMT-GPTR models with more components in tensor factorization (e.g., sMT-GPR(15,10)) identify more localized defects. Considering the fact that the probabilities are averaged across subjects, this may reflect averaging over patterns that are more heterogeneous across individuals.

4 Related Work

Hyun *et al.* introduced spatial [14] and spatio-temporal [15] Gaussian predictive process to model neuroimaging data. They used functional principal component analysis to approximate the spatial/temporal covariance matrix of the random effect combined with a multivariate autoregressive model for the noise. Their approach focuses on point estimation of outputs and does not provide a practical solution to estimate predictive uncertainty, thus cannot be employed for normative modeling. Our TGPP framework resolves this issue, and further, due to its flexible and general tensor assumption on the data structure, can be extended to other dimensions of neuroimaging data (e.g., modalities).

Shvartsman *et al.* [28] reformulated common fMRI analysis methods, such as representational similarity analysis in matrix-variate normal models resulting in a unified framework for fMRI data analysis. They theoretically and experimentally showed the potentials of matrix-normal assumption

⁴Plots are created using the Nilearn toolbox [1].

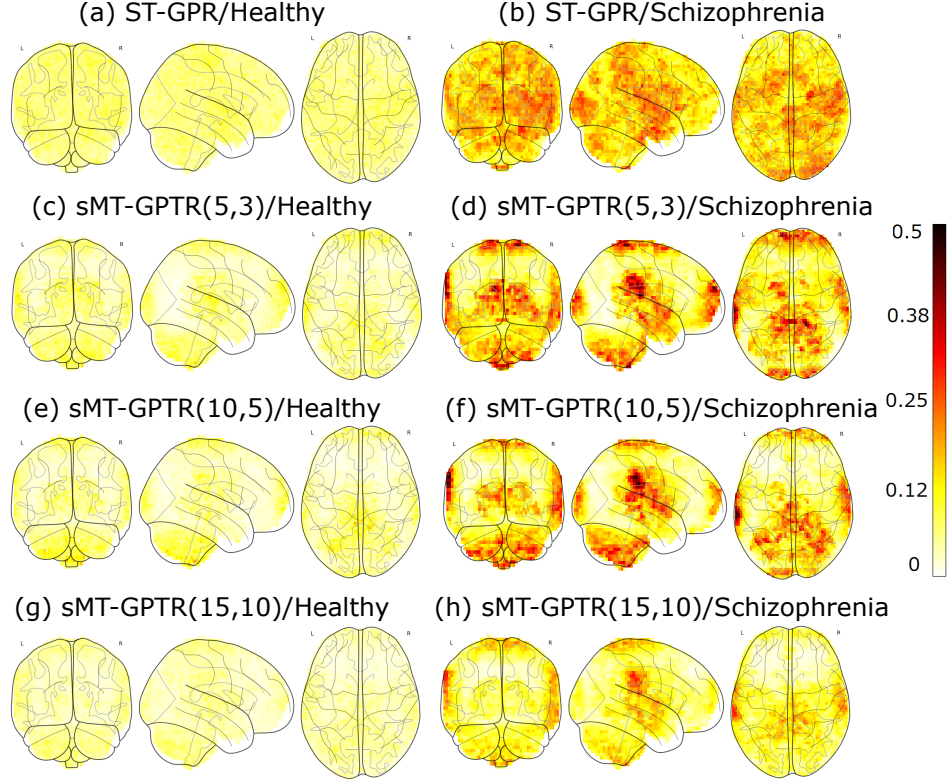


Figure 2: The probability of each voxel to deviate from the normative model in healthy and Schizophrenia populations; derived by ST-GPR and sMR-GPTR with different component numbers.

on fMRI data in simultaneously modeling spatial and temporal noise covariances. Although our aim is different, our tensor-variate normal assumption on the distribution of the random-effect and noise can be seen as an extension of their approach, extending theoretical concepts in the multi-way modeling of neuroimaging data from 2-dimensional matrix-structured data to D -dimensional tensors.

The idea of exploiting Kronecker algebra to scale up GPR for multi-way data is well studied in machine learning [27, 33, 32, 11]. However, all these methods are developed to deal with multi-way *input* data (*i.e.*, single-task learning), whereas we extend these ideas to multi-way *output* data (*i.e.*, multi-task learning).

5 Summary, Limitation, and Future Work

In this study, assuming a tensor-variate normal distribution on multi-way neuroimaging data and in a novel tensor Gaussian predictive process framework, we introduced a scalable multi-task Gaussian process tensor regression approach to model multi-way structured random-effect and noise on very high-dimensional neuroimaging data. The proposed approach provides a breakthrough toward practical modeling different sources of variations across different dimensions of large neuroimaging cohorts. On a clinical fMRI dataset, we exemplified one possible application of the proposed method for normative modeling of spatially distributed effects at the whole-brain level. We demonstrated that our framework provides more accurate results with reasonable computational costs, and it focuses better on the core underlying brain abnormalities relative to a mass-univariate alternative. Due to its tensor-based design, the presented TGPP framework needs full-grid data across space, and/or other possible dimensions of neuroimaging data. This can be considered as a possible limitation when dealing with data with missing values across some data dimensions. One possible future direction is to solve this problem by imputing the grid using imaginary observations [33, 32]. For future work, we aim to better understand the neuroscientific basis for the performance improvements we report (*e.g.*, across multiple model orders and using different representations of the normative probability maps) and will apply the proposed method to very large cohorts in order to provide a more comprehensive model of biological variation across the population.

References

- [1] Alexandre Abraham, Fabian Pedregosa, Michael Eickenberg, Philippe Gervais, Andreas Mueller, Jean Kossaifi, Alexandre Gramfort, Bertrand Thirion, and Gael Varoquaux. Machine learning for neuroimaging with scikit-learn. *Frontiers in Neuroinformatics*, 8:14, 2014.
- [2] Mauricio Alvarez and Neil D Lawrence. Sparse convolved Gaussian processes for multi-output regression. In *Advances in neural information processing systems*, pages 57–64, 2009.
- [3] Mauricio A Álvarez and Neil D Lawrence. Computationally efficient convolved multiple output Gaussian processes. *Journal of Machine Learning Research*, 12:1459–1500, 2011.
- [4] Mauricio A Alvarez, David Luengo, Michalis K Titsias, and Neil D Lawrence. Efficient multioutput Gaussian processes through variational inducing kernels. In *International Conference on Artificial Intelligence and Statistics*, pages 25–32, 2010.
- [5] Edwin V Bonilla, Kian M Chai, and Christopher Williams. Multi-task Gaussian process prediction. In *Advances in neural information processing systems*, pages 153–160, 2008.
- [6] F. DuBois Bowman, Brian Caffo, Susan Spear Bassett, and Clinton Kilts. A bayesian hierarchical framework for spatial modeling of fMRI data. *NeuroImage*, 39(1):146 – 156, 2008.
- [7] Anthony C Davison and Raphaël Huser. Statistics of extremes. *Annual Review of Statistics and Its Application*, 2(1):203–235, 2015.
- [8] Lucy Foulkes and Sarah-Jayne Blakemore. Studying individual differences in human adolescent brain development. *Nature neuroscience*, page 1, 2018.
- [9] Karl J Friston, Andrew P Holmes, CJ Price, C Büchel, and KJ Worsley. Multisubject fMRI Studies and Conjunction Analyses. *NeuroImage*, 10(4):385 – 396, 1999.
- [10] Ke Gao and John P Harrison. Tensor variate normal distribution for stress variability analysis. *Rock Mechanics and Rock Engineering: From the Past to the Future*, page 119, 2016.
- [11] Elad Gilboa, Yunus Saatçi, and John P Cunningham. Scaling Multidimensional Inference for Structured Gaussian Processes. *IEEE Transactions on Pattern Analysis and Machine Intelligence*, 37(2):424–436, Feb 2015.
- [12] Krzysztof J Gorgolewski, Joke Durnez, and Russell A Poldrack. Preprocessed consortium for neuropsychiatric phenomics dataset [version 2; referees: 2 approved]. *F1000Research*, 6(1262), 2017.
- [13] Caterina Gratton, Timothy O Laumann, Ashley N Nielsen, Deanna J Greene, Evan M Gordon, Adrian W Gilmore, Steven M Nelson, Rebecca S Coalson, Abraham Z Snyder, Bradley L Schlaggar, et al. Functional brain networks are dominated by stable group and individual factors, not cognitive or daily variation. *Neuron*, 98(2):439–452, 2018.
- [14] Jung Won Hyun, Yimei Li, John H. Gilmore, Zhaohua Lu, Martin Styner, and Hongtu Zhu. Sgpp: spatial gaussian predictive process models for neuroimaging data. *NeuroImage*, 89:70 – 80, 2014.
- [15] Jung Won Hyun, Yimei Li, Chao Huang, Martin Styner, Weili Lin, and Hongtu Zhu. Stgp: Spatio-temporal gaussian process models for longitudinal neuroimaging data. *NeuroImage*, 134:550 – 562, 2016.
- [16] Shitij Kapur, Anthony G Phillips, and Thomas R Insel. Why has it taken so long for biological psychiatry to develop clinical tests and what to do about it? *Molecular psychiatry*, 17(12):1174, 2012.
- [17] Alex Kendall and Yarin Gal. What uncertainties do we need in bayesian deep learning for computer vision? In *Advances in Neural Information Processing Systems*, pages 5580–5590, 2017.
- [18] Tamara G. Kolda and Brett W. Bader. Tensor decompositions and applications. *SIAM Review*, 51(3):455–500, 2009.
- [19] Jean Kossaifi, Yannis Panagakis, and Maja Pantic. Tensorly: Tensor learning in python. *arXiv preprint arXiv:1610.09555*, 2016.
- [20] Charles F. Van Loan. The ubiquitous kronecker product. *Journal of Computational and Applied Mathematics*, 123(1):85 – 100, 2000.
- [21] Andre F Marquand, Iead Rezek, Jan Buitelaar, and Christian F Beckmann. Understanding heterogeneity in clinical cohorts using normative models: beyond case-control studies. *Biological psychiatry*, 80(7):552–561, 2016.
- [22] Reza Mirnezami, Jeremy Nicholson, and Ara Darzi. Preparing for Precision Medicine. *New England Journal of Medicine*, 366(6):489–491, 2012. PMID: 22256780.
- [23] Buchsbaum MS and Rieder RO. Biologic heterogeneity and psychiatric research: Platelet mao activity as a case study. *Archives of General Psychiatry*, 36(11):1163–1169, 1979.
- [24] Morten Mørup. Applications of tensor (multiway array) factorizations and decompositions in data mining. *Wiley Interdisciplinary Reviews: Data Mining and Knowledge Discovery*, 1(1):24–40, 2011.

- [25] Russell A Poldrack, Eliza Congdon, William Triplett, KJ Gorgolewski, KH Karlsgodt, JA Mumford, FW Sabb, NB Freimer, ED London, TD Cannon, et al. A phenome-wide examination of neural and cognitive function. *Scientific data*, 3:160110, 2016.
- [26] Barbara Rakitsch, Christoph Lippert, Karsten Borgwardt, and Oliver Stegle. It is all in the noise: Efficient multi-task Gaussian process inference with structured residuals. In *Advances in neural information processing systems*, pages 1466–1474, 2013.
- [27] Yunus Saatçi. *Scalable inference for structured Gaussian process models*. PhD thesis, University of Cambridge, 2012.
- [28] Michael Shvartsman, Narayanan Sundaram, Mikio C Aoi, Adam Charles, Theodore C Wilke, and Jonathan D Cohen. Matrix-normal models for fMRI analysis. In *Proceedings of the 22th International Conference on Artificial Intelligence and Statistics*. PMLR, 2018.
- [29] Oliver Stegle, Christoph Lippert, Joris M Mooij, Neil D Lawrence, and Karsten M Borgwardt. Efficient inference in matrix-variate gaussian models with iid observation noise. In *Advances in neural information processing systems*, pages 630–638, 2011.
- [30] Ledyard R Tucker. Some mathematical notes on three-mode factor analysis. *Psychometrika*, 31(3):279–311, 1966.
- [31] Christopher KI Williams and Carl Edward Rasmussen. Gaussian processes for regression. In *Advances in neural information processing systems*, pages 514–520, 1996.
- [32] Andrew Wilson and Hannes Nickisch. Kernel Interpolation for Scalable Structured Gaussian Processes (KISS-GP). In Francis Bach and David Blei, editors, *Proceedings of the 32nd International Conference on Machine Learning*, volume 37 of *Proceedings of Machine Learning Research*, pages 1775–1784, Lille, France, 07–09 Jul 2015. PMLR.
- [33] Andrew G Wilson, Elad Gilboa, Arye Nehorai, and John P Cunningham. Fast kernel learning for multidimensional pattern extrapolation. In *Advances in Neural Information Processing Systems*, pages 3626–3634, 2014.
- [34] Thomas Wolfers, Jan K. Buitelaar, Christian F. Beckmann, Barbara Franke, and Andre F. Marquand. From estimating activation locality to predicting disorder: A review of pattern recognition for neuroimaging-based psychiatric diagnostics. *Neuroscience and Biobehavioral Reviews*, 57:328 – 349, 2015.
- [35] Thomas Wolfers, Daan van Rooij, Jaap Oosterlaan, Dirk Heslenfeld, Catharina A. Hartman, Pieter J. Hoekstra, Christian F. Beckmann, Barbara Franke, Jan K. Buitelaar, and Andre F. Marquand. Quantifying patterns of brain activity: Distinguishing unaffected siblings from participants with adhd and healthy individuals. *NeuroImage: Clinical*, 12:227 – 233, 2016.
- [36] Mark William Woolrich, Timothy Edward John Behrens, Christian F Beckmann, and Stephen M Smith. Mixture models with adaptive spatial regularization for segmentation with an application to fMRI data. *IEEE Transactions on Medical Imaging*, 24(1):1–11, Jan 2005.

Supplementary Materials

Throughout the supplementary materials we use the same notation introduced in the main text.

Useful Equations

For $\mathbf{A} \in \mathbb{R}^{M \times N}$, $\mathbf{B} \in \mathbb{R}^{P \times Q}$, and \mathbf{C}, \mathbf{D} (with appropriate size) we have:

1. $\mathbf{A} = \mathbf{U}_\mathbf{A} \mathbf{S}_\mathbf{A} \mathbf{U}_\mathbf{A}^\top$ is the eigenvalue decomposition of \mathbf{A} ,
2. $(\mathbf{A}\mathbf{C}\mathbf{B})^{-1} = \mathbf{B}^{-1}\mathbf{C}^{-1}\mathbf{A}^{-1}$,
3. $(\mathbf{A} \otimes \mathbf{B})(\mathbf{C} \otimes \mathbf{D}) = \mathbf{A}\mathbf{C} \otimes \mathbf{B}\mathbf{D}$,
4. $(\mathbf{A} \otimes \mathbf{B})^{-1} = \mathbf{A}^{-1} \otimes \mathbf{B}^{-1}$,
5. the eigenvalue decomposition of $\mathbf{A} \otimes \mathbf{B} + \mathbf{I}$ is: $(\mathbf{U}_\mathbf{A} \otimes \mathbf{U}_\mathbf{B})(\mathbf{S}_\mathbf{A} \otimes \mathbf{S}_\mathbf{B} + \mathbf{I})(\mathbf{U}_\mathbf{A}^\top \otimes \mathbf{U}_\mathbf{B}^\top)$,
6. $(\mathbf{A} \otimes \mathbf{B})\text{vec}(\mathbf{C}) = \text{vec}(\mathbf{B}\mathbf{C}\mathbf{A}^\top)$,
7. $\ln |\mathbf{A}\mathbf{C}| = \ln(|\mathbf{A}| |\mathbf{C}|) = \ln |\mathbf{A}| + \ln |\mathbf{C}|$,
8. for $\mathbf{C} \in \mathbb{R}^{N \times N}$, $\frac{d}{dx} \ln |\mathbf{C}| = \text{Tr}[\mathbf{C}^{-1} \frac{d\mathbf{C}}{dx}]$,
9. $\text{Tr}[\mathbf{A}\mathbf{C}\mathbf{B}\mathbf{D}] = \text{Tr}[\mathbf{C}\mathbf{B}\mathbf{D}\mathbf{A}] = \text{Tr}[\mathbf{B}\mathbf{D}\mathbf{A}\mathbf{C}] = \text{Tr}[\mathbf{D}\mathbf{A}\mathbf{C}\mathbf{B}]$,
10. $\text{Tr}[\mathbf{A}^\top \mathbf{C}] = \text{vec}(\mathbf{C})^\top \text{vec}(\mathbf{A})$,
11. $\ln |\mathbf{C} \otimes \mathbf{D}| = M \ln |\mathbf{C}| + N \ln |\mathbf{D}|$, for $\mathbf{C} \in \mathbb{R}^{N \times N}$, $\mathbf{D} \in \mathbb{R}^{M \times M}$,
12. $\ln |\text{diag}(\mathbf{C})| = \prod_{i=1}^N \mathbf{C}[i, i]$, for $\mathbf{C} \in \mathbb{R}^{N \times N}$.

Tensor Normal Distribution for \mathcal{Z}'

Eq. 5 is derived as follows:

$$\begin{aligned}
 p(\mathcal{Z}' \mid \mathbf{C}_i \big|_{i=1}^D, \mathbf{R}) &= \mathcal{TN}(\mathbf{0}, \bigotimes_{i=1}^D \mathbf{C}_i \otimes \mathbf{R}) = \frac{\exp(-\frac{1}{2} \text{vec}(\mathcal{Z}')^\top [\bigotimes_{i=1}^D \mathbf{C}_i \otimes \mathbf{R}]^{-1} \text{vec}(\mathcal{Z}'))}{\sqrt{(2\pi)^N \prod_{i=1}^D P_i \left| \bigotimes_{i=1}^D \mathbf{C}_i \right|^{\prod_{i=1}^D P_i} |\mathbf{R}|^N}} = \\
 &= \frac{\exp(-\frac{1}{2} \text{vec}(\mathcal{Z}')^\top \text{vec}(\mathbf{R}^{-1} \mathbf{Z}'_{(1)} \bigotimes_{i=1}^D \mathbf{C}_i^{-1}))}{\sqrt{(2\pi)^N \prod_{i=1}^D P_i \left| \bigotimes_{i=1}^D \mathbf{C}_i \right|^{\prod_{i=1}^D P_i} |\mathbf{R}|^N}} = \frac{\exp(-\frac{1}{2} \text{Tr}[\bigotimes_{i=1}^D \mathbf{C}_i^{-1} \mathbf{Z}'_{(1)}^\top \mathbf{R}^{-1} \mathbf{Z}'_{(1)}])}{\sqrt{(2\pi)^N \prod_{i=1}^D P_i \left| \bigotimes_{i=1}^D \mathbf{C}_i \right|^{\prod_{i=1}^D P_i} |\mathbf{R}|^N}} \\
 &\xrightarrow{\mathbf{Z}'_{(1)} = \hat{\mathbf{Z}}_{(1)} (\bigotimes_{i=1}^D \mathbf{B}_i^\top)^{-1}} \frac{\exp(-\frac{1}{2} \text{Tr}[\bigotimes_{i=1}^D \mathbf{C}_i^{-1} \bigotimes_{i=1}^D \mathbf{B}_i^\dagger \hat{\mathbf{Z}}_{(1)}^\top \mathbf{R}^{-1} \hat{\mathbf{Z}}_{(1)} (\bigotimes_{i=1}^D \mathbf{B}_i^\top)^{-1}])}{\sqrt{(2\pi)^N \prod_{i=1}^D P_i \left| \bigotimes_{i=1}^D \mathbf{C}_i \right|^{\prod_{i=1}^D P_i} |\mathbf{R}|^N}} = \\
 &= \frac{\exp(-\frac{1}{2} \text{Tr}[\bigotimes_{i=1}^D \mathbf{B}_i \mathbf{C}_i^{-1} \mathbf{B}_i^\top \hat{\mathbf{Z}}_{(1)}^\top \mathbf{R}^{-1} \hat{\mathbf{Z}}_{(1)}])}{\sqrt{(2\pi)^N \prod_{i=1}^D P_i \left| \bigotimes_{i=1}^D \mathbf{C}_i \right|^{\prod_{i=1}^D P_i} |\mathbf{R}|^N}}.
 \end{aligned}$$

Efficient Mean Prediction

Eq. 10(a) is derived from Eq. 9(a) as follows:

$$\begin{aligned}
\text{vec}(\mathcal{M}^*) &= (\bigotimes_{i=1}^D \mathbf{B}_i \mathbf{C}_i \mathbf{B}_i^\top \otimes \mathbf{R}^*) (\bigotimes_{i=1}^D \mathbf{B}_i \mathbf{C}_i \mathbf{B}_i^\top \otimes \mathbf{R} + \bigotimes_{i=1}^D \mathbf{\Lambda}_i \mathbf{\Sigma}_i \mathbf{\Lambda}_i^\top \otimes \mathbf{\Omega})^{-1} \text{vec}(\mathcal{Y}) \\
&= (\bigotimes_{i=1}^D \mathbf{B}_i \mathbf{C}_i \mathbf{B}_i^\top \otimes \mathbf{R}^*) (\bigotimes_{i=1}^D \mathbf{B}_i \mathbf{C}_i \mathbf{B}_i^\top \otimes \mathbf{R} + \bigotimes_{i=1}^D \mathbf{\Lambda}_i \mathbf{U}_{\Sigma_i} \mathbf{S}_{\Sigma_i}^\top \mathbf{U}_{\Sigma_i}^\top \mathbf{\Lambda}_i^\top \otimes \mathbf{U}_{\Omega} \mathbf{S}_{\Omega} \mathbf{U}_{\Omega}^\top)^{-1} \text{vec}(\mathcal{Y}) \\
&= (\bigotimes_{i=1}^D \mathbf{B}_i \mathbf{C}_i \mathbf{B}_i^\top \otimes \mathbf{R}^*) (\bigotimes_{i=1}^D \mathbf{\Lambda}_i \mathbf{U}_{\Sigma_i} \mathbf{S}_{\Sigma_i}^{-0.5} \otimes \mathbf{U}_{\Omega} \mathbf{S}_{\Omega}^{-0.5}) (\bigotimes_{i=1}^D \tilde{\mathbf{C}}_i \otimes \tilde{\mathbf{R}} + \mathbf{I})^{-1} \\
&\quad (\bigotimes_{i=1}^D \mathbf{S}_{\Sigma_i}^{-0.5} \mathbf{U}_{\Sigma_i}^\top \mathbf{\Lambda}_i^\top \otimes \mathbf{S}_{\Omega}^{-0.5} \mathbf{U}_{\Omega}^\top) \text{vec}(\mathcal{Y}) \\
&= (\bigotimes_{i=1}^D \mathbf{B}_i \mathbf{C}_i \mathbf{B}_i^\top \mathbf{\Lambda}_i \mathbf{U}_{\Sigma_i} \mathbf{S}_{\Sigma_i}^{-0.5} \otimes \mathbf{R}^* \mathbf{U}_{\Omega} \mathbf{S}_{\Omega}^{-0.5}) (\bigotimes_{i=1}^D \mathbf{U}_{\tilde{\mathbf{C}}_i} \otimes \mathbf{U}_{\tilde{\mathbf{R}}}) (\bigotimes_{i=1}^D \mathbf{S}_{\tilde{\mathbf{C}}_i} \otimes \mathbf{S}_{\tilde{\mathbf{R}}} + \mathbf{I})^{-1} \\
&\quad (\bigotimes_{i=1}^D \mathbf{U}_{\tilde{\mathbf{C}}_i}^\top \otimes \mathbf{U}_{\tilde{\mathbf{R}}}^\top) \text{vec}(\mathbf{S}_{\Omega}^{-0.5} \mathbf{U}_{\Omega}^\top \mathbf{Y}_{(1)}) (\bigotimes_{i=1}^D \mathbf{\Lambda}_i \mathbf{U}_{\Sigma_i} \mathbf{S}_{\Sigma_i}^{-0.5}) \\
&= (\bigotimes_{i=1}^D \mathbf{B}_i \mathbf{C}_i \mathbf{B}_i^\top \mathbf{\Lambda}_i \mathbf{U}_{\Sigma_i} \mathbf{S}_{\Sigma_i}^{-0.5} \otimes \mathbf{R}^* \mathbf{U}_{\Omega} \mathbf{S}_{\Omega}^{-0.5}) (\bigotimes_{i=1}^D \mathbf{U}_{\tilde{\mathbf{C}}_i} \otimes \mathbf{U}_{\tilde{\mathbf{R}}}) \text{vec}(\tilde{\mathbf{Y}}) \\
&= (\bigotimes_{i=1}^D \mathbf{B}_i \mathbf{C}_i \mathbf{B}_i^\top \mathbf{\Lambda}_i \mathbf{U}_{\Sigma_i} \mathbf{S}_{\Sigma_i}^{-0.5} \otimes \mathbf{R}^* \mathbf{U}_{\Omega} \mathbf{S}_{\Omega}^{-0.5}) \text{vec}(\mathbf{U}_{\tilde{\mathbf{R}}} \tilde{\mathbf{Y}} \bigotimes_{i=1}^D \mathbf{U}_{\tilde{\mathbf{C}}_i}^\top) \\
&= \mathbf{R}^* \mathbf{U}_{\Omega} \mathbf{S}_{\Omega}^{-0.5} \mathbf{U}_{\tilde{\mathbf{R}}} \tilde{\mathbf{Y}} \bigotimes_{i=1}^D \mathbf{U}_{\tilde{\mathbf{C}}_i}^\top \mathbf{S}_{\Sigma_i}^{-0.5} \mathbf{U}_{\Sigma_i}^\top \mathbf{\Lambda}_i^\top \mathbf{B}_i \mathbf{C}_i \mathbf{B}_i^\top \quad .
\end{aligned}$$

Efficient Variance Prediction

Eq. 10(b) is derived from Eq. 9(b) as follows:

$$\begin{aligned}
\mathbf{V}^* &= \left(\bigotimes_{i=1}^D \mathbf{B}_i \mathbf{C}_i \mathbf{B}_i^\top \otimes \mathbf{R}^{**} \right) - \left(\bigotimes_{i=1}^D \mathbf{B}_i \mathbf{C}_i \mathbf{B}_i^\top \otimes \mathbf{R}^* \right) \left(\bigotimes_{i=1}^D \mathbf{B}_i \mathbf{C}_i \mathbf{B}_i^\top \otimes \mathbf{R} + \bigotimes_{i=1}^D \mathbf{\Lambda}_i \mathbf{\Sigma}_i \mathbf{\Lambda}_i^\top \otimes \mathbf{\Omega} \right)^{-1} \\
&\quad \left(\bigotimes_{i=1}^D \mathbf{B}_i \mathbf{C}_i \mathbf{B}_i^\top \otimes \mathbf{R}^{*\top} \right) \\
&= \left(\bigotimes_{i=1}^D \mathbf{B}_i \mathbf{C}_i \mathbf{B}_i^\top \otimes \mathbf{R}^{**} \right) - \left(\bigotimes_{i=1}^D \mathbf{B}_i \mathbf{C}_i \mathbf{B}_i^\top \otimes \mathbf{R}^* \right) \left(\bigotimes_{i=1}^D \mathbf{\Lambda}_i \mathbf{U}_{\Sigma_i} \mathbf{S}_{\Sigma_i}^{-0.5} \otimes \mathbf{U}_{\Omega} \mathbf{S}_{\Omega}^{-0.5} \right) \\
&\quad \left(\bigotimes_{i=1}^D \tilde{\mathbf{C}}_i \otimes \tilde{\mathbf{R}} + \mathbf{I} \right)^{-1} \left(\bigotimes_{i=1}^D \mathbf{S}_{\Sigma_i}^{-0.5} \mathbf{U}_{\Sigma_i}^\top \mathbf{\Lambda}_i^\top \otimes \mathbf{S}_{\Omega}^{-0.5} \mathbf{U}_{\Omega}^\top \right) \left(\bigotimes_{i=1}^D \mathbf{B}_i \mathbf{C}_i \mathbf{B}_i^\top \otimes \mathbf{R}^{*\top} \right) \\
&= \left(\bigotimes_{i=1}^D \mathbf{B}_i \mathbf{C}_i \mathbf{B}_i^\top \otimes \mathbf{R}^{**} \right) - \left(\bigotimes_{i=1}^D \mathbf{B}_i \mathbf{C}_i \mathbf{B}_i^\top \mathbf{\Lambda}_i \mathbf{U}_{\Sigma_i} \mathbf{S}_{\Sigma_i}^{-0.5} \otimes \mathbf{R}^* \mathbf{U}_{\Omega} \mathbf{S}_{\Omega}^{-0.5} \right) \\
&\quad \left(\bigotimes_{i=1}^D \mathbf{U}_{\tilde{\mathbf{C}}_i} \otimes \mathbf{U}_{\tilde{\mathbf{R}}} \right) \left(\bigotimes_{i=1}^D \mathbf{S}_{\tilde{\mathbf{C}}_i} \otimes \mathbf{S}_{\tilde{\mathbf{R}}} + \mathbf{I} \right)^{-1} \left(\bigotimes_{i=1}^D \mathbf{U}_{\tilde{\mathbf{C}}_i}^\top \otimes \mathbf{U}_{\tilde{\mathbf{R}}}^\top \right) \left(\bigotimes_{i=1}^D \mathbf{S}_{\Sigma_i}^{-0.5} \mathbf{U}_{\Sigma_i}^\top \mathbf{\Lambda}_i^\top \mathbf{B}_i \mathbf{C}_i \mathbf{B}_i^\top \otimes \mathbf{S}_{\Omega}^{-0.5} \mathbf{U}_{\Omega}^\top \mathbf{R}^{*\top} \right) \\
&= \left(\bigotimes_{i=1}^D \mathbf{B}_i \mathbf{C}_i \mathbf{B}_i^\top \otimes \mathbf{R}^{**} \right) - \left(\bigotimes_{i=1}^D \mathbf{B}_i \mathbf{C}_i \mathbf{B}_i^\top \mathbf{\Lambda}_i \mathbf{U}_{\Sigma_i} \mathbf{S}_{\Sigma_i}^{-0.5} \mathbf{U}_{\tilde{\mathbf{C}}_i} \otimes \mathbf{R}^* \mathbf{U}_{\Omega} \mathbf{S}_{\Omega}^{-0.5} \mathbf{U}_{\tilde{\mathbf{R}}} \right) \\
&\quad \left(\bigotimes_{i=1}^D \mathbf{S}_{\tilde{\mathbf{C}}_i} \otimes \mathbf{S}_{\tilde{\mathbf{R}}} + \mathbf{I} \right)^{-1} \left(\bigotimes_{i=1}^D \mathbf{U}_{\tilde{\mathbf{C}}_i}^\top \mathbf{S}_{\Sigma_i}^{-0.5} \mathbf{U}_{\Sigma_i}^\top \mathbf{\Lambda}_i^\top \mathbf{B}_i \mathbf{C}_i \mathbf{B}_i^\top \otimes \mathbf{U}_{\tilde{\mathbf{R}}}^\top \mathbf{S}_{\Omega}^{-0.5} \mathbf{U}_{\Omega}^\top \mathbf{R}^{*\top} \right) .
\end{aligned}$$

Efficient Log Marginal Likelihood Evaluation

Eq. 11 is derived as follows:

$$\begin{aligned}
L &= -\frac{NT}{2} \ln(2\pi) - \frac{1}{2} \ln |\mathbf{K}| - \frac{1}{2} \text{vec}(\mathbf{Y})^\top \mathbf{K}^{-1} \text{vec}(\mathbf{Y}) \\
&= -\frac{NT}{2} \ln(2\pi) - \frac{1}{2} \ln \left| \bigotimes_{i=1}^D \mathbf{B}_i \mathbf{C}_i \mathbf{B}_i^\top \otimes \mathbf{R} + \bigotimes_{i=1}^D \mathbf{\Lambda}_i \mathbf{\Sigma}_i \mathbf{\Lambda}_i^\top \otimes \mathbf{\Omega} \right| - \\
&\quad \frac{1}{2} \text{vec}(\mathbf{Y})^\top \left(\bigotimes_{i=1}^D \mathbf{B}_i \mathbf{C}_i \mathbf{B}_i^\top \otimes \mathbf{R} + \bigotimes_{i=1}^D \mathbf{\Lambda}_i \mathbf{\Sigma}_i \mathbf{\Lambda}_i^\top \otimes \mathbf{\Omega} \right)^{-1} \text{vec}(\mathbf{Y}) \\
&= -\frac{NT}{2} \ln(2\pi) - \frac{1}{2} \ln \left| \left(\bigotimes_{i=1}^D \mathbf{\Lambda}_i \mathbf{U}_{\Sigma_i} \mathbf{S}_{\Sigma_i}^{-0.5} \otimes \mathbf{U}_{\Omega} \mathbf{S}_{\Omega}^{-0.5} \right) \left(\bigotimes_{i=1}^D \tilde{\mathbf{C}}_i \otimes \tilde{\mathbf{R}} + \mathbf{I} \right)^{-1} \left(\bigotimes_{i=1}^D \mathbf{S}_{\Sigma_i}^{-0.5} \mathbf{U}_{\Sigma_i}^\top \mathbf{\Lambda}_i^\top \otimes \mathbf{S}_{\Omega}^{-0.5} \mathbf{U}_{\Omega}^\top \right) \right| - \\
&\quad \frac{1}{2} \text{vec}(\mathbf{Y})^\top \left[\left(\bigotimes_{i=1}^D \mathbf{\Lambda}_i \mathbf{U}_{\Sigma_i} \mathbf{S}_{\Sigma_i}^{-0.5} \otimes \mathbf{U}_{\Omega} \mathbf{S}_{\Omega}^{-0.5} \right) \left(\bigotimes_{i=1}^D \tilde{\mathbf{C}}_i \otimes \tilde{\mathbf{R}} + \mathbf{I} \right)^{-1} \left(\bigotimes_{i=1}^D \mathbf{S}_{\Sigma_i}^{-0.5} \mathbf{U}_{\Sigma_i}^\top \mathbf{\Lambda}_i^\top \otimes \mathbf{S}_{\Omega}^{-0.5} \mathbf{U}_{\Omega}^\top \right) \right] \text{vec}(\mathbf{Y}) \\
&= -\frac{NT}{2} \ln(2\pi) - \frac{1}{2} \ln \left| \bigotimes_{i=1}^D \mathbf{\Lambda}_i \mathbf{U}_{\Sigma_i} \mathbf{S}_{\Sigma_i} \mathbf{U}_{\Sigma_i}^\top \mathbf{\Lambda}_i^\top \otimes \mathbf{U}_{\Omega} \mathbf{S}_{\Omega} \mathbf{U}_{\Omega}^\top \right| - \frac{1}{2} \ln \left| \bigotimes_{i=1}^D \mathbf{S}_{\tilde{\mathbf{C}}_i} \otimes \mathbf{S}_{\tilde{\mathbf{R}}} + \mathbf{I} \right| \\
&\quad - \frac{1}{2} \text{vec}(\mathbf{S}_{\Omega}^{-0.5} \mathbf{U}_{\Omega}^\top \mathbf{Y}_{(1)} \bigotimes_{i=1}^D \mathbf{\Lambda}_i \mathbf{U}_{\Sigma_i} \mathbf{S}_{\Sigma_i}^{-0.5})^\top \left(\bigotimes_{i=1}^D \mathbf{U}_{\tilde{\mathbf{C}}_i} \otimes \mathbf{U}_{\tilde{\mathbf{R}}} \right) \left(\bigotimes_{i=1}^D \mathbf{S}_{\tilde{\mathbf{C}}_i} \otimes \mathbf{S}_{\tilde{\mathbf{R}}} + \mathbf{I} \right)^{-1} \\
&\quad \left(\bigotimes_{i=1}^D \mathbf{U}_{\tilde{\mathbf{C}}_i}^\top \otimes \mathbf{U}_{\tilde{\mathbf{R}}}^\top \right) \text{vec}(\mathbf{S}_{\Omega}^{-0.5} \mathbf{U}_{\Omega}^\top \mathbf{Y}_{(1)} \bigotimes_{i=1}^D \mathbf{\Lambda}_i \mathbf{U}_{\Sigma_i} \mathbf{S}_{\Sigma_i}^{-0.5}) \\
&= -\frac{NT}{2} \ln(2\pi) - \frac{1}{2} \ln \left| \bigotimes_{i=1}^D \mathbf{S}_{\Sigma_i} \otimes \mathbf{S}_{\Omega} \right| - \frac{1}{2} \ln \left| \bigotimes_{i=1}^D \mathbf{S}_{\tilde{\mathbf{C}}_i} \otimes \mathbf{S}_{\tilde{\mathbf{R}}} + \mathbf{I} \right| - \frac{1}{2} \text{vec}(\mathbf{Y}')^\top \left(\bigotimes_{i=1}^D \mathbf{S}_{\tilde{\mathbf{C}}_i} \otimes \mathbf{S}_{\tilde{\mathbf{R}}} + \mathbf{I} \right)^{-1} \text{vec}(\mathbf{Y}') \\
&= -\frac{NT}{2} \ln(2\pi) - \frac{N}{2} \sum_{j=1}^T (\ln \bigotimes_{i=1}^D \mathbf{S}_{\Sigma_i})[j, j] - \frac{T}{2} \sum_{j=1}^N (\ln \mathbf{S}_{\Omega}[j, j]) - \frac{1}{2} \\
&\quad \sum_{k=1}^T \sum_{j=1}^N \ln \left(\bigotimes_{i=1}^D \mathbf{S}_{\tilde{\mathbf{C}}_i}[k, k] \mathbf{S}_{\tilde{\mathbf{R}}}[j, j] + 1 \right) - \frac{1}{2} \text{vec}(\mathbf{Y}')^\top \left(\bigotimes_{i=1}^D \mathbf{S}_{\tilde{\mathbf{C}}_i} \otimes \mathbf{S}_{\tilde{\mathbf{R}}} + \mathbf{I} \right)^{-1} \text{vec}(\mathbf{Y}') .
\end{aligned}$$

Derivatives of L with Respect to Parameters

In the optimization process, the derivatives of L with respect to $\theta_{\mathbf{C}_i} \in \Theta_{\mathbf{C}_i}$, $\theta_{\Sigma_i} \in \Theta_{\Sigma_i}$, $\theta_{\mathbf{R}} \in \Theta_{\mathbf{R}}$, and $\theta_{\Omega} \in \Theta_{\Omega}$ can be efficiently computed as follows:

Gradients of L with Respect to $\theta_{\mathbf{C}_i}$

$$\begin{aligned}
\frac{\partial L}{\partial \theta_{\mathbf{C}_i}} &= -\frac{1}{2} \text{diag} \left(\left(\bigotimes_{k=1}^D \mathbf{S}_{\tilde{\mathbf{C}}_k} \otimes \mathbf{S}_{\tilde{\mathbf{R}}} + \mathbf{I} \right)^{-1} \right)^\top \\
&\quad \text{diag}(\mathbf{S}_{\tilde{\mathbf{C}}_1} \otimes \mathbf{S}_{\tilde{\mathbf{C}}_2} \otimes \cdots \otimes \mathbf{U}_{\tilde{\mathbf{C}}_1}^\top \mathbf{S}_{\Sigma_1}^{-0.5} \mathbf{U}_{\Sigma_1}^\top \mathbf{\Lambda}_1^\top \mathbf{B}_1 \frac{\partial \mathbf{C}_1}{\partial \theta_{\tilde{\mathbf{C}}_1}} \mathbf{B}_1^\top \mathbf{\Lambda}_1 \mathbf{U}_{\Sigma_1} \mathbf{S}_{\Sigma_1}^{-0.5} \mathbf{U}_{\tilde{\mathbf{C}}_1} \otimes \cdots \otimes \mathbf{S}_{\tilde{\mathbf{C}}_D} \otimes \mathbf{S}_{\tilde{\mathbf{R}}}) \\
&\quad + \frac{1}{2} \text{vec}(\tilde{\mathbf{Y}})^\top \text{vec}(\mathbf{S}_{\tilde{\mathbf{R}}} \tilde{\mathbf{Y}} (\mathbf{S}_{\tilde{\mathbf{C}}_1} \otimes \mathbf{S}_{\tilde{\mathbf{C}}_2} \otimes \cdots \otimes \mathbf{U}_{\tilde{\mathbf{C}}_1}^\top \mathbf{S}_{\Sigma_1}^{-0.5} \mathbf{U}_{\Sigma_1}^\top \mathbf{\Lambda}_1^\top \mathbf{B}_1 \frac{\partial \mathbf{C}_1}{\partial \theta_{\tilde{\mathbf{C}}_1}} \mathbf{B}_1^\top \mathbf{\Lambda}_1 \mathbf{U}_{\Sigma_1} \mathbf{S}_{\Sigma_1}^{-0.5} \mathbf{U}_{\tilde{\mathbf{C}}_1} \otimes \cdots \otimes \mathbf{S}_{\tilde{\mathbf{C}}_D})),
\end{aligned}$$

Gradients of L with Respect to θ_{Σ_i}

$$\begin{aligned} \frac{\partial L}{\partial \theta_{\Sigma_i}} = & -\frac{1}{2} \text{diag}((\bigotimes_{k=1}^D \mathbf{S}_{\tilde{\Sigma}_k} \otimes \mathbf{S}_{\tilde{\Omega}} + \mathbf{I})^{-1})^\top \\ & \text{diag}(\mathbf{S}_{\tilde{\Sigma}_1} \otimes \mathbf{S}_{\tilde{\Sigma}_2} \otimes \cdots \otimes \mathbf{U}_{\tilde{\Sigma}_i}^\top \mathbf{S}_{\mathbf{C}_i}^{-0.5} \mathbf{U}_{\mathbf{C}_i}^\top \mathbf{B}_i^\top \mathbf{A}_i \frac{\partial \Sigma_i}{\partial \theta_{\Sigma_i}} \mathbf{A}_i^\top \mathbf{B}_i \mathbf{U}_{\mathbf{C}_i} \mathbf{S}_{\mathbf{C}_i}^{-0.5} \mathbf{U}_{\tilde{\Sigma}_i} \otimes \cdots \otimes \mathbf{S}_{\tilde{\Sigma}_D} \otimes \mathbf{S}_{\tilde{\Omega}}) \\ & + \frac{1}{2} \text{vec}(\tilde{\mathbf{Y}})^\top \text{vec}(\mathbf{S}_{\tilde{\Omega}} \tilde{\mathbf{Y}} (\mathbf{S}_{\tilde{\Sigma}_1} \otimes \mathbf{S}_{\tilde{\Sigma}_2} \otimes \cdots \otimes \mathbf{U}_{\tilde{\Sigma}_i}^\top \mathbf{S}_{\mathbf{C}_i}^{-0.5} \mathbf{U}_{\mathbf{C}_i}^\top \mathbf{B}_i^\top \mathbf{A}_i \frac{\partial \Sigma_i}{\partial \theta_{\Sigma_i}} \mathbf{A}_i^\top \mathbf{B}_i \mathbf{U}_{\mathbf{C}_i} \mathbf{S}_{\mathbf{C}_i}^{-0.5} \mathbf{U}_{\tilde{\Sigma}_i} \otimes \cdots \otimes \mathbf{S}_{\tilde{\Sigma}_D})), \end{aligned}$$

The derivation of the determinant and squared terms of $\frac{\partial L}{\partial \theta_{\Sigma_i}}$ are similar to those of $\frac{\partial L}{\partial \theta_{\mathbf{C}_i}}$.

Gradients of L with Respect to $\theta_{\mathbf{R}}$:

$$\begin{aligned} \frac{\partial L}{\partial \theta_{\mathbf{R}}} = & -\frac{1}{2} \text{diag}((\bigotimes_{k=1}^D \mathbf{S}_{\tilde{\mathbf{C}}_k} \otimes \mathbf{S}_{\tilde{\mathbf{R}}} + \mathbf{I})^{-1})^\top \text{diag}(\bigotimes_{k=1}^D \mathbf{S}_{\tilde{\mathbf{C}}_k} \otimes \mathbf{U}_{\tilde{\mathbf{R}}}^\top \mathbf{S}_{\tilde{\Omega}}^{-0.5} \mathbf{U}_{\tilde{\Omega}}^\top \frac{\partial \mathbf{R}}{\partial \theta_{\mathbf{R}}} \mathbf{U}_{\tilde{\Omega}} \mathbf{S}_{\tilde{\Omega}}^{-0.5} \mathbf{U}_{\tilde{\mathbf{R}}}) \\ & + \frac{1}{2} \text{vec}(\tilde{\mathbf{Y}})^\top \text{vec}(\mathbf{U}_{\tilde{\mathbf{R}}}^\top \mathbf{S}_{\tilde{\Omega}}^{-0.5} \mathbf{U}_{\tilde{\Omega}}^\top \frac{\partial \mathbf{R}}{\partial \theta_{\mathbf{R}}} \mathbf{U}_{\tilde{\Omega}} \mathbf{S}_{\tilde{\Omega}}^{-0.5} \mathbf{U}_{\tilde{\mathbf{R}}} \tilde{\mathbf{Y}} \bigotimes_{k=1}^D \mathbf{S}_{\tilde{\mathbf{C}}_k}). \end{aligned}$$

The derivation of the determinant and squared terms of $\frac{\partial L}{\partial \theta_{\mathbf{R}}}$ are similar to those of $\frac{\partial L}{\partial \theta_{\mathbf{C}_i}}$.

Gradients of L with Respect to θ_{Ω} :

$$\begin{aligned} \frac{\partial L}{\partial \theta_{\Omega}} = & -\frac{1}{2} \text{diag}((\bigotimes_{k=1}^D \mathbf{S}_{\tilde{\Sigma}_k} \otimes \mathbf{S}_{\tilde{\Omega}} + \mathbf{I})^{-1})^\top \text{diag}(\bigotimes_{k=1}^D \mathbf{S}_{\tilde{\Sigma}_k} \otimes \mathbf{U}_{\tilde{\Omega}}^\top \mathbf{S}_{\tilde{\mathbf{R}}}^{-0.5} \mathbf{U}_{\tilde{\mathbf{R}}}^\top \frac{\partial \Omega}{\partial \theta_{\Omega}} \mathbf{U}_{\tilde{\mathbf{R}}} \mathbf{S}_{\tilde{\mathbf{R}}}^{-0.5} \mathbf{U}_{\tilde{\Omega}}) \\ & + \frac{1}{2} \text{vec}(\tilde{\mathbf{Y}})^\top \text{vec}(\mathbf{U}_{\tilde{\Omega}}^\top \mathbf{S}_{\tilde{\mathbf{R}}}^{-0.5} \mathbf{U}_{\tilde{\mathbf{R}}}^\top \frac{\partial \Omega}{\partial \theta_{\Omega}} \mathbf{U}_{\tilde{\mathbf{R}}} \mathbf{S}_{\tilde{\mathbf{R}}}^{-0.5} \mathbf{U}_{\tilde{\Omega}} \tilde{\mathbf{Y}} \bigotimes_{k=1}^D \mathbf{S}_{\tilde{\Sigma}_k}). \end{aligned}$$

The procedure to derive the determinant and squared terms of $\frac{\partial L}{\partial \theta_{\Omega}}$ is similar to $\frac{\partial L}{\partial \theta_{\mathbf{C}_i}}$.

Comparing the Regression Performance

This figure summarizes the average regression performance (R^2) across all voxels for benchmarked approaches. All methods show similar performance in terms of the quality of regression. Note that the low R^2 values are due to averaging over all voxels that many are irrelevant to regressors in \mathbf{X} .

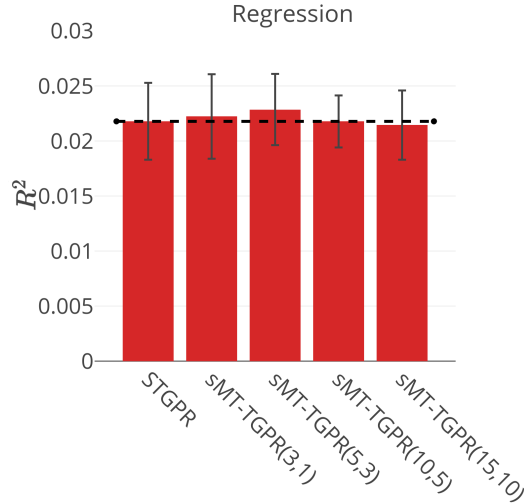


Figure 3: Comparison between ST-GPR and sMT-GPTR in terms of their regression performance.